RSC Advances

ROYAL SOCIETY OF CHEMISTRY

www.rsc.org/advances

Multicolor nanoprobes based on silica-coated gadolinium oxide nanoparticles with highly reduced toxicity

Timur Sh. Atabaev[1*], Jong Ho Lee[2], Dong-Wook Han[2], Ki Seok Choo[3], Ung Bae Jeon[3], Jae Yeon Hwang[3], Jeong A Yeom[3], ChulHee Kang[4], Hyung-Kook Kim[1*], Yoon-Hwae Hwang[1*]

1. Department of Nano Energy Engineering and BK21 Plus Nanoconvergence Technology Division, Pusan National University, Miryang 627-706, Republic of Korea

2. Department of Cogno-Mechatronics Engineering, Pusan National University, Busan 609-735, Republic of Korea

3. Department of Radiology, Pusan National University Yangsan Hospital, Yangsan 626-770, Republic of Korea

4. Department of Chemistry, Washington State University, Pullman, WA 99164-4630, USA

Corresponding authors: timuratabaev@yahoo.com (T.S. Atabaev), hkkim@pusan.ac.kr (H.K. Kim) and yhwang@pusan.ac.kr (Y. H. Hwang)

Abstract:

In recent years, multimodal contrast agents have attracted considerable attention in biomedical imaging. This paper reports the development of a multimodal nanoprobe based on silica-coated gadolinium oxide nanoparticles (NPs) for T_1-enhanced magnetic resonance (MR) and multicolor optical imaging. MR relaxivity measurements showed that these core-shell NPs could generate strong positive contrast enhancement in T_1-weighted MR imaging (MRI). Owing to the nominally co-doped Eu^{3+} and Tb^{3+} ions in the Gd_2O_3 host, the synthesized nanoprobes could simultaneously emit blue, green and red fluorescence signals. Furthermore, the cytotoxicity results showed that a thin silica coating on the surface of gadolinium oxide NPs could increase the biocompatibility of the fabricated nanoprobes considerably. The excellent multicolor fluorescence and MRI functionalities of these nanoprobes could have potential biomedical applications.

Keywords: Contrast agents, Gadolinium oxide, Nanoprobes, Core-shell structure

Introduction

Rapid developments in nanotechnology have allowed the preparation of systems with previously unknown properties, thereby expanding the area of their applications. Novel nanomaterials with multimodal functionalities have significant importance for their potential applications in simultaneous diagnosis and therapy [1]. Among the different nanomaterials, gadolinium-based contrast agents are interesting because the seven unpaired electrons in its valence orbitals lead to one of the highest magnetic moments of all elements. The Gd-based contrast agent brightens the image where it is present ("positive" contrast agent), because it has a significant impact on the longitudinal relaxivity but a limited impact on the transverse relaxivity. On the other hand, most Gd-based chelates currently used in clinics are unsuitable for optical cellular imaging. Furthermore, they are also poorly ingested and retained by cells [2]. Therefore, new multimodal imaging nanoprobes with different imaging modalities need to be developed for more accurate imaging and diagnosis.

Gadolinium oxide NPs might be a good candidate because they can have larger longitudinal R_1 relaxivity values than commercially available Gd-based chelates because of their higher density of magnetic ions [3, 4]. The exceptional relaxometric characteristics of ultrafine gadolinia-based suspensions allow the tracking of cells with T_1-weighted MRI sequences without compromising the resolution [5]. In addition, gadolinium oxide can also be used as an excellent host matrix for a range of optically-active lanthanides for optical imaging [3, 6]. As an ideal nanoprobe, gadolinium oxide-based NPs must meet at least four requirements: (a) NPs should be nontoxic for biomedical applications, (b) NPs should be colloidally stable in a range of solutions, (c) the surface of NPs can be modified easily using substances with specificity, and (d) NPs can be detected easily with different imaging techniques. In this regard, bare gadolinium oxide NPs show high toxicity towards cells, tissues and organs. Therefore, suitable surface modification of gadolinium oxide NPs is needed to make them nontoxic and biocompatible. Among some inorganic materials tested, a silica matrix is a good candidate as a biocoating [7]. For example, a uniform silica coating can reduce the potential toxicity of the bare gadolinium oxide NPs. In

addition, an inert silica coating prevents the agglomeration of NPs and can be surface-functionalized easily with specific functional groups [8, 9].

This study examined the dual contrast imaging capability of prepared silica-coated Gd_2O_3:Tb^{3+},Eu^{3+} NPs. Bioinert silica was used as a surface coating to make the gadolinia NPs biocompatible, colloidally-stable and suitable for surface-functionalization. To demonstrate the potential of prepared Gd_2O_3:Tb^{3+},Eu^{3+}@SiO_2 NPs for medical imaging, the magnetic resonance water proton relaxivities, cellular uptake and *in-vitro* cellular cytotoxicity were investigated. Owing to the presence of nominally co-doped Eu^{3+} and Tb^{3+} ions in the Gd_2O_3 host, these NPs could be applied potentially to multicolor optical imaging, making this system a dual-mode nanoprobe.

Experimental details

Sample preparation

Analytical grade Gd_2O_3 (99.99 %), Eu_2O_3 (99.99 %), Tb_2O_3 (99.99 %), HNO_3 (70.0 %), urea (99.0-100.5%), tetraethyl orthosilicate TEOS (98.0 %), and ammonium hydroxide solution (28.0-30.0%) were purchased from Sigma-Aldrich and used as received. Spherical Gd_2O_3 NPs co-doped with Tb^{3+} and Eu^{3+} were fabricated using a urea homogeneous precipitation method using the reported protocols [10, 11]. At the first stage, a sealed beaker with a freshly prepared aqueous solution of rare-earth nitrates (0.001 mol in 40 ml of H_2O) was placed into an electrical furnace and heated to 90 °C for 1.5 h. The dried synthesized precipitates were then calcined in air at 800 °C for 1 h to produce the oxide NPs. At the second stage, a beaker containing the dispersed gadolinia NPs (10 mg) in cyclohexane/ethanol mixture (45/5 ml) was stirred for 10 min and 0.2 ml ammonium hydroxide was added to form a transparent solution. Finally, 0.1 ml TEOS was added and the reaction was cotinued for 4 h with vigorous stirring. The prepared nanoprobes were collected by centrifugation, followed by the dialysis in deionized ultrapure water for 12 h to eliminate the unreacted products. The resulting core-shell nanoprobes were then calcined in air at 300 °C for 1 h.

Characterization

The structure of the prepared powders was examined by XRD (Bruker D8 Discover) using Cu-Kα radiation (λ = 0.15405 nm) at a 2θ scan range 20–60° 2θ. The morphology of the particles was characterized by field emission transmission electron microscopy (FETEM, JEOL JEM-2100F). Hydrodynamic sizes and zeta potentials of the obtained nanoprobes were measured performed using a Nano ZS Zetasizer (Malvern Instruments Ltd). The measurements were repeated three times to obtain an average value. The structural properties of the prepared samples were analyzed by Fourier transform infrared (FTIR, Jasco FT/IR6300) spectroscopy. The magnetic measurements were performed by a quantum design vibrating sample magnetometer (QD-VSM on a PPMS 6000 machine). The photoluminescence PL measurements were performed using a Hitachi F-7000 spectrophotometer equipped with a 150 W Xenon lamp as the excitation source. The T_1-weighted images were obtained using a 1.5 T MRI scanner (Siemens) using the T_1-weighted spin-echo method [TR/TE = 500 ms/15 ms, field of view (FOV) = 100 mm × 100 mm, slice thickness = 2 mm, matrix = 256 × 204, number of excitations (NEX) = 2]. All measurements were performed at a room temperature of 22 ± 1 °C.

Cell culture and cytotoxicity assay

A murine fibroblast cell line (L-929 cells from subcutaneous connective tissue) was obtained from the American Type Culture Collection (ATCC CCL-1[TM], Rockville, MD). The cells were routinely maintained in Dulbecco's modified Eagle's medium (Sigma-Aldrich), supplemented with 10% fetal bovine serum (Sigma-Aldrich) and 1% antibiotic antimycotic solution (including 10 000 units penicillin, 10 mg streptomycin and 25 mg amphotericin B per ml, Sigma-Aldrich) at 37 °C in 95% humidity and 5% CO_2. The number of viable cells was indirectly quantified using highly water-soluble tetrazolium salt [WST-8,2-(2-methoxy-4-nitrophenyl)-3-(4-nitrophenyl)-5-(2,4-disulfophenyl)-2*H*-tetrazolium, monosodium salt] (Dojindo Lab., Kumamoto, Japan), reduced to a water-soluble formazan dye by mitochondrial dehydrogenases. The cell viability was found to be directly proportional to the metabolic reaction products obtained in WST-8. Briefly, the WST-8 assay was conducted as follows. L-929 cells were treated with increasing concentration (0–500 ppm) of nanoprobes and then incubated with WST-8 for the last 4 h of the culture periods (24 h) at 37 °C in the dark. Parallel sets of wells containing freshly cultured nontreated cells were regarded as negative controls. The absorbance was determined to be 450

nm using an ELISA reader (SpectraMax[®] 340, Molecular Device Co., Sunnyvale, CA). The relative cell viability was determined as the percentage ratio of the optical densities in the medium (containing the nanoprobes at each concentration) to that of the fresh control medium.

Fluorescence microscopy

To examine the cellular uptake and distribution of nanoprobes within the L-929 cells and subsequent cell imaging, the cells were treated with 50 ppm of nanoprobes for 24 h. After treatment, the cells were fixed with 3.5% paraformaldehyde (Sigma-Aldrich) in 0.1 M phosphate buffer (pH = 7) for 10 min at room temperature and immediately observed under a fluorescence microscope (IX81-F72, Olympus Optical, Osaka, Japan).

Statistical analysis

All variables were tested in three independent cultures for cytotoxicity assay, which was repeated twice (n = 6). Quantitative data are expressed as the mean ± standard deviation (SD). Data were tested for homogeneity of variances using the test of Levene, prior to statistical analysis. Statistical comparisons were carried out by a one-way analysis of variance (ANOVA), followed by a Bonferroni test for multiple comparisons. A value of $p < 0.05$ was considered statistically significant.

Results and discussion

The multicolor nanoprobes were fabricated by co-doping with Tb^{3+} and Eu^{3+} in the same gadolinia host matrix. The Eu^{3+} concentration was kept at 0.2 mol.%, whereas the Tb^{3+} concentration was 1 mol.%. FETEM and DLS were used to examine the morphology and size distributions of the prepared samples. Figure 1 shows that the uncoated sample consisted of well-dispersed NPs with a size distribution of 68±18 nm. These multicolor nanoprobes were coated with a thin silica shell layer, as shown in the core-shell structure Fig 1a (Inset). The thin silica shells had a mean thickness of ~18 nm. After the silica coating, the spherical morphology of the core-shell nanoprobes was retained except for the larger particles size (102 ± 21 nm). The mean diameters of the samples, as measured by DLS (Figure 1b), before and after the silica shell

coating were in accordance with the estimated sizes from FETEM analysis. In addition, zeta potential was measured at pH 7.4 to ensure the stability of the prepared nanoprobes. Measurements reveal that zeta potential of uncoated nanoprobes is around 6 mV, whereas, zeta potential value of silica-coated nanoprobes is -28 mV. Thus, silica-coated nanoprobes with higher (negative) zeta potential demonstrate better colloidal stability (Figure S1, Supplementary Information).
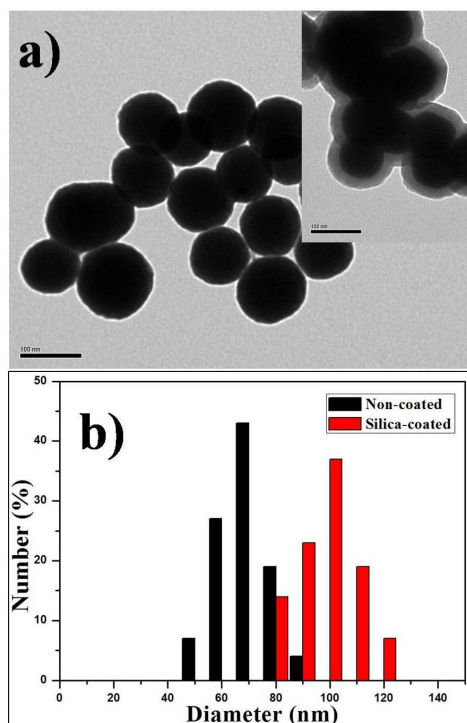
Fig. 1. (a) FETEM images of the non-coated nanoprobes (Inset image is silica-coated nanoprobes, scale bar - 100 nm) , (b) size distribution measurements for non-coated and silica-coated nanoprobes

Fourier transform infrared (FTIR) spectroscopy and X-ray diffraction (XRD) revealed the structural properties of the prepared nanoprobes. Figure 2 shows that in both cases, the samples exhibited the characteristic stretching vibration peaks of Gd-O at ~540 cm^{-1} [3, 12]. The

characteristic Si-O-Si peak in the spectrum, at approximately $\sim$1109 cm^{-1}, was clearly observed only in the case of the silica-coated sample [13]. Moreover, the silica-coated sample exhibited some additional bands, i.e., angular deformation of water molecules ($\sim$1660 cm^{-1}) and the stretching vibrations of the OH group ($\sim$3600 cm^{-1}). This confirmed the successful silica shell formation because silica can adsorbs some water from the air. XRD peaks for both samples could be assigned easily to the standard cubic Gd_2O_3 structure (JCPDS no. 88-2165), which belongs to the *Ia*3 (206) space group (Figure 2, inset) [6, 13]. No additional peaks from the co-dopants were detected because of their relatively low doping concentration. The appearance of a broad XRD peak at low diffraction angles highlights the amorphous silica coating in the case of the silica-coated sample. In addition, magnetic measurements showed that both samples clearly show typical paramagnetic behavior (Figure S2, Supplementary Information). However, due to a dielectric nature of the silica shell layer, the paramagnetic properties of silica-coated sample is slightly lower than that of the bare sample.
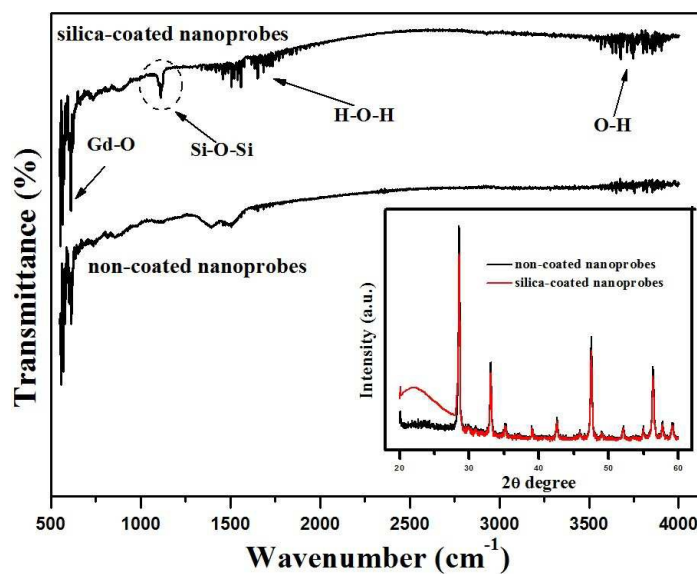
Fig. 2. Normalized FTIR spectra for the prepared nanoprobes (Inset image is typical X-ray diffraction patterns for the prepared nanoprobes)

The prepared samples were examined further at room-temperature by PL under 300 nm continuous excitation. In both cases, the PL emission spectra consisted of several distinguishable *f-f* transitions within the doped Tb^{3+} and Eu^{3+}. For example, the blue emission within the range of 478-507 nm, corresponds to the characteristic $^5D_4{\rightarrow}^7F_6$ transition of Tb^{3+}. The strong green band with a maximum at 543 nm is another characteristic $^5D_4{\rightarrow}^7F_5$ transition of Tb^{3+}. The red peak centered at 612 nm was due to the strong energy transfer from Tb^{3+} to Eu^{3+} [14, 15] and assigned to the characteristic $^5D_0{\rightarrow}^7F_2$ transition of Eu^{3+}. The weak yellow-near-red band in the range, 577-603 nm, appeared due to the mixture of different signals ($^5D_4{\rightarrow}^7F_4$ of Tb^{3+} and $^5D_0{\rightarrow}^7F_0$ + $^5D_0{\rightarrow}^7F_1$ of Eu^{3+}). This shows that one can easily obtain a multicolor nanoprobe by co-doping Tb^{3+} and Eu^{3+} in the Gd_2O_3 matrix.
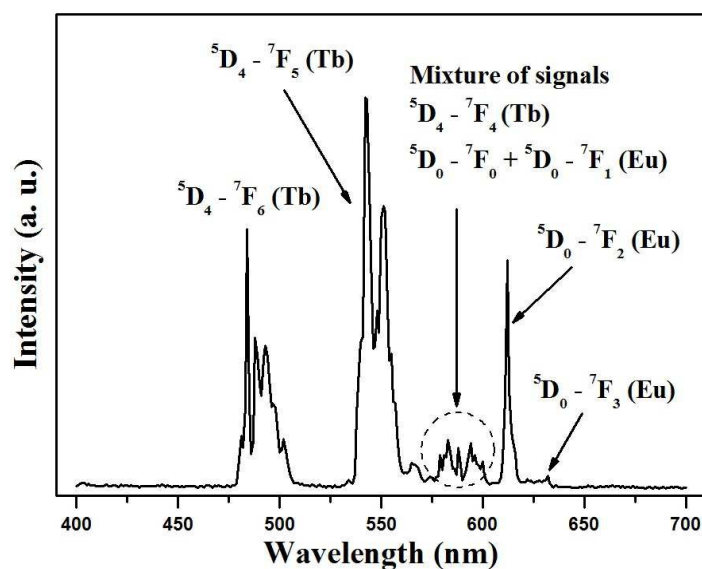
Fig. 3. PL emission spectra for the silica-coated nanoprobes

To demonstrate the safety of the prepared samples for biomedical imaging applications, it is essential to measure their cytotoxicity. As shown in Figure 4, the cytotoxicity profiles of the prepared samples in L-929 fibroblastic cells were determined using a WST-8 assay. The cells exposed to increasing concentrations (0-500 ppm) of the prepared samples for 24 h showed a noticeable dose-dependent decrease in their relative cell viability. The uncoated sample began to

induce a slight decrease in cell viability from ~8 ppm. However, the cell viability was significantly ($p < 0.05$) decreased at concentrations higher than 125 ppm. On the other hand, the silica-coated sample caused no significant decrease in cell viability at much higher concentrations ~125 ppm. These dose-dependent responses of the L-929 cells to the samples were also evident from morphological observations (Figure S3, Supplementary Information). According to the "Trojan horse" mechanism [16], metal ions from the uncoated sample can generate reactive oxygen species in the cell interior, leading to oxidative stress to living cells. The biocompatible silica shell layer coating can partially block this interaction, which leads to a better biocompatibility of the samples [17]. Therefore, considering the *in-vitro* cytotoxicity only, it can be concluded that silica-coated particles can be used safely for bio-imaging at doses lower than ~125 ppm.
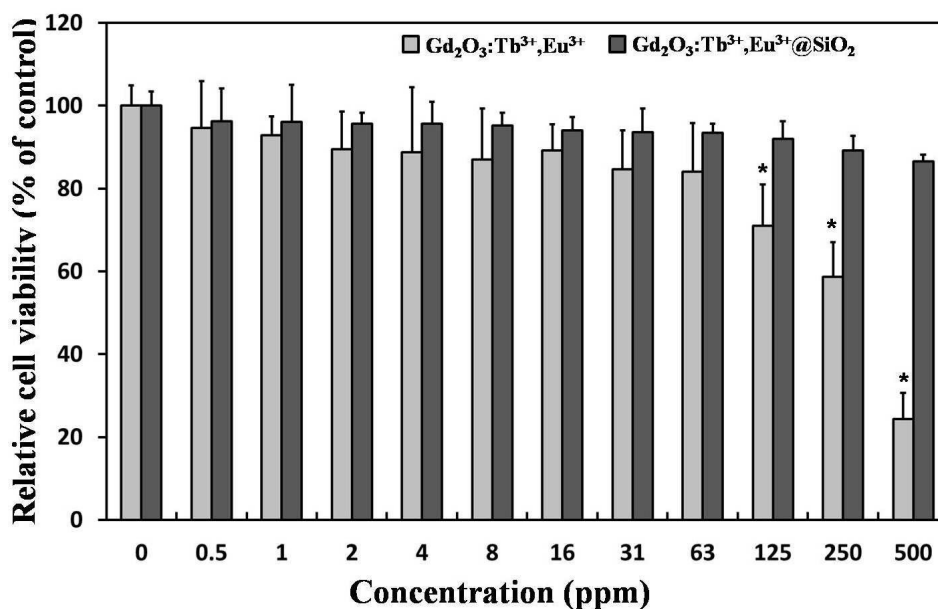
Fig. 4. Relative cell viability of L-929 cells exposed for 24 h to increasing concentrations (0-500 ppm) of prepared samples with and without silica shell coating. An asterisk ($*$) denotes a significant difference compared with the control, $p < 0.05$.

The silica-coated sample, which showed better biocompatibility, was used for further experiments. A 1.5 T clinical MRI scanner was utilized further to demonstrate the potential of the silica-coated nanoprobes for T_1-weighted MR imaging. Figure 5 (inset) shows that the T_1-relaxation time of the water protons was reduced significantly, and the T_1-weighted images became brighter with increasing concentration of the silica-coated nanoprobes. The slope of the linear fit of $1/T_1$ vs. silica-coated nanoprobes concentration yielded a longitudinal relaxivity (R_1) of 4.73 ± 0.11. This value is slightly higher than that commercially available Gd-chelates (e.g. Gd-DTPA, Gd-DOTA, etc.) [18]. Therefore, the synergic magnetism of multiple Gd^{3+} ions concentrated within each single nanoparticle can enhance the relaxivity rates significantly. Therefore, better tissue contrast will be possible when nanoprobes with a high local concentration of magnetic ions accumulate within the intra-cellular region.
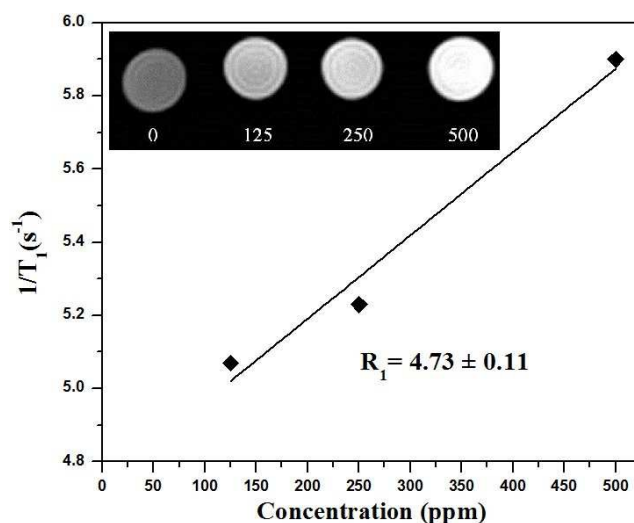
Fig. 5. Longitudinal relaxivity rate R_1 *versus* various concentrations of silica-coated nanoprobes measured at room-temperature. Inset is T_1-weighted images of the silica-coated nanoprobes at various concentrations.

To demonstrate the multicolor imaging potential of the silica-coated nanoprobes, a cultured monolayer of L-929 cells was incubated for 4 h in the culture medium with a nanoprobe suspension at a concentration of 50 ppm. Figure 6 shows that the L-929 cells grow with normal

fibroblast-like morphologies after labeling with the silica-coated nanoprobes (Phase contrast). The fluorescence images (DAPI, FITC and TRITC) showed that silica-coated nanoprobes can emit intense blue, green and red colors simultaneously, as confirmed by PL measurements. Therefore, these nanoprobes can make molecular cell imaging, tracking and targeting possible through internalization and wide distribution inside the cells (pinocytosis or nonspecific endocytosis mechanisms) [19, 20]. Furthermore, this also suggests that these multicolor nanoprobes allow the integration of two molecular imaging technique, such as high resolution molecular fluorescence imaging and non-invasive deep-tissue MR imaging.
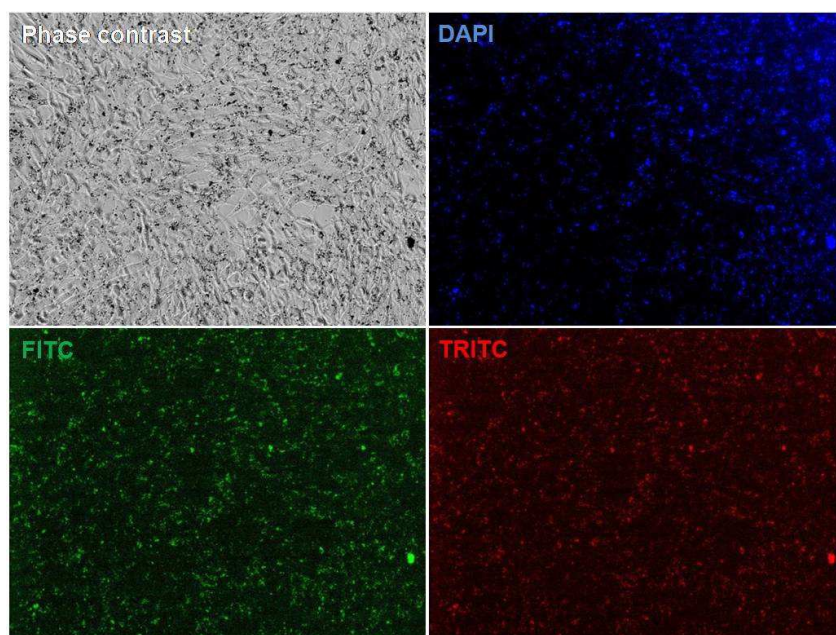
Fig. 6. Multicolor fluorescence micrograps of L-929 cells treated with 50 ppm of silica-coated nanoprobes.

Conclusion

Multicolor lanthanide-based nanoprobes were developed for the molecular imaging of living cells using fluorescence and MRI technique. The morphology, structural and optical properties of these nanoprobes were examined by FETEM, FTIR, XRD, and PL spectroscopy, respectively. The co-doping of Eu^{3+} and Tb^{3+} resulted in strong multicolor fluorescence emission, whereas the paramagnetic properties of the host Gd_2O_3 material were used for T_1-weighted MR imaging.

Cytotoxicity studies showed that a thin silica coating on the surface of nanoprobes is quite favorable, because it can strongly reduce the toxic effects of bare nanoprobes in living cells. Therefore, by combining the merits of the fluorescent and paramagnetic properties, these nanoprobes have potential applications in the development of nanosized contrast agents.

Acknowledgements

References

1. O.S. Wolfbeis, *Chem. Soc. Rev.* 2015, **44**, 4743-4768.

2. L. Faucher, Y. Gossuin, A. Hocq, M.A. Fortin, *Nanotechnology* 2011, **22**, 295103.

3. T.S. Atabaev, J.H. Lee, D.W. Han, H.K. Kim, Y.H. Hwang, *RSC Adv.* 2014, 4, 34343-34349.

4. T.S. Atabaev, J.H. Lee, D.W. Han, H.K. Kim, Y.H. Hwang, *J. Adv. Ceram.* 2015, 4, 118-122

5. S. Setua, D. Menon, A. Asok, S. Nair, M. Koyakutty, *Biomaterials* 2010, 31, 714-729

6. T.S. Atabaev, Z. Piao, Y.H. Hwang, H.K. Kim, N.H. Hong, *J. Alloys Compd.* 2013, 572, 113-117

7. T.S. Atabaev, J.H. Lee, J.H. Lee, D.W. Han, Y.H. Hwang, H.K. Kim, N.H. Hong, *Nanotechnology* 2013, 24, 345603

8. T.S. Atabaev, G. Urmanova, M. Ajmal, N.H. Hong, *BioNanoSci.* 2013, 3, 132-136

9. T.S. Atabaev, G. Urmanova, N.H. Hong, *Nano Life* 2014, 4, 1441003

10. T.S. Atabaev, J.H. Lee, D.W. Han, Y.H. Hwang, H.K. Kim, *J. Biomed Mater. Res. Part A* 2012, 100, 2287-2294

11. T.S. Atabaev, H.K. Kim, Y.H. Hwang, *Nanoscale Res. Lett.* 2013, 8, 357

12. G. Jia, H. You, K. Liu, Y. Zheng, N. Guo, H. Zhang, *Langmuir* 2010, 26, 5122-5128

13. Q. Zhang, C. Chen, M. Wang, J. Cai, J. Xu, C. Xia, *Nanoscale Res. Lett.* 2011, 6, 586

14. D. Tu, Y. Liang, R. Liu, D. Li, *J. Lumin.* 2011, 131, 2569-2573

15. T.S. Atabaev, H.K. Kim, Y.H. Hwang, *J. Colloid Interface Sci.* 2012, 373, 14-19

16. L. Thrall, *Environ. Sci. Technol.* 2007, 41, 3791-3792

17. T.S. Atabaev, O.S. Jin, J.H. Lee, D.W. Han, H.H.T. Vu, Y.H. Hwang, H.K. Kim, *RSC Adv.* 2012, 2, 9495-9501

18. L. Faucher, M. Tremblay, J. Lagueux, Y. Gossuin, M.-A. Fortin, *ACS Appl. Mater. Interfaces* 2012, 4, 4506-4515

19. A. L. Doiron, B. Clarck, K. D. Rinker, *Biotechnol. Bioeng.* 2011, 108, 2988-2998

20. W. Jiang, B. Y. Kim, J. T. Rutka, W. C. Chan, *Nat. Nanotechnol.* 2008, 3, 145-150

230x92mm (150 x 150 DPI)